Kibble-Zurek mechanism in a quenched ferromagnetic Bose-Einstein condensate

Hiroki Saito,[1] Yuki Kawaguchi,[2] and Masahito Ueda[2,3]
[1]*Department of Applied Physics and Chemistry, The University of Electro-Communications, Tokyo 182-8585, Japan*
[2]*Department of Physics, Tokyo Institute of Technology, Tokyo 152-8551, Japan*
[3]*ERATO Macroscopic Quantum Control Project, JST, Tokyo 113-8656, Japan*
(Received 11 April 2007; published 12 October 2007)

It is shown that spin vortices are created through the Kibble-Zurek mechanism in the quantum phase transition of a spin-1 ferromagnetic Bose-Einstein condensate when the applied magnetic field is quenched to below a critical value. It is also shown that the spin correlation functions have finite correlation lengths, and that the magnetization at widely separated positions grows in random directions, resulting in spontaneous creation of spin vortices. We numerically confirm the scaling laws that the winding number of spin vortices is proportional to the square root of the length of a closed path and, for a slow quench, is proportional to $\tau_{\mathrm{Q}}^{-1/6}$ with τ_{Q} being the quench time. The relevance of spin conservation to the Kibble-Zurek mechanism is discussed.

DOI: 10.1103/PhysRevA.76.043613 PACS number(s): 03.75.Mn, 03.75.Lm, 73.43.Nq, 64.60.Ht

I. INTRODUCTION

Spontaneous symmetry breaking in phase transitions can produce local domains of an order parameter. If these domains are separated by a great distance such that they cannot exchange information, the local domains initially grow with random phases and eventually give rise to topological defects when they overlap. This scenario of topological-defect formation in continuous-symmetry breaking is known as the Kibble-Zurek (KZ) mechanism [1,2]. The mechanism was originally proposed to predict cosmic-string and monopole formation in the early Universe [1] and has since been applied to a wide variety of systems. The KZ mechanism has been experimentally studied in liquid crystals [3,4], superfluid ^{4}He [5] and ^{3}He [6,7], an optical Kerr medium [8], Josephson junctions [9,10], and superconducting films [11].

Spontaneous magnetization in a spinor Bose-Einstein condensate (BEC) has recently attracted broad interest as a new system for studying the KZ mechanism [12–15]. In an experiment performed by the Berkeley group [12], a BEC of $F=1$ ^{87}Rb atoms was prepared in the $m=0$ state, where F is the hyperfine spin and m is its projection in the direction of the magnetic field. By quenching the magnetic field, say in the z direction, magnetization appears in the x-y plane. Since the spinor Hamiltonian is axisymmetric with respect to the z axis, magnetization in the x-y plane breaks the U(1) symmetry in the spin space. Thus local domain formation can be expected to lead to topological defects, i.e., spin vortices, through the KZ mechanism.

Another mechanism for spin-vortex creation in spontaneous magnetization of a spinor BEC is dynamical instability [16]. In Ref. [13], we have performed numerical simulations for the same parameters as those in the Berkeley experiment [12] and found that the main experimental results can be explained by dynamical instability triggered by residual atoms in the $m=\pm 1$ components. Moreover, as shown in Fig. 3(b) in Ref. [12], the spin correlation function oscillates and extends over at least several tens of μm. To realize a situation where the KZ mechanism applies, in which magnetic domains should grow independently, the size of the system must be much larger than the spin correlation length and there must be no residual $m=\pm 1$ atoms in the initial state. The aim of the present paper is to show that under these conditions spin vortices are generated through the KZ mechanism.

In the present paper we will consider one-dimensional (1D)-ring and two-dimensional (2D)-disk geometries. We will show that for a 1D ring, the average spin winding number after a quench is proportional to the square root of the circumference of the ring, which is in agreement with the KZ prediction [2]. For a 2D disk, the winding number along a path of radius R is proportional to $R^{1/2}$ as long as R is much larger than the vortex spacing, while it is proportional to R for small R. When the magnetic field is quenched slowly, the winding number is shown to be proportional to $\tau_{\mathrm{Q}}^{-1/6}$, with τ_{Q} being the quench time. This power law can be explained by Zurek's simple discussion [2].

The spinor BEC is different from other systems in which the KZ mechanism has been observed, in that the total spin is conserved when the quadratic Zeeman energy q is negligible. This fact is apparently incompatible with the KZ postulate, since the magnetic domains must be correlated with each other so that the total magnetization vanishes. We will show that for $q=0$, small magnetic domains are aligned so as to cancel out the local spin when averaged over the correlation length, and that they are independent of each other over a greater length scale. The spin conservation is thus compatible with the KZ postulate of independent growth of magnetization.

The present paper is organized as follows. Section II analyzes the spontaneous magnetization of a spin-1 BEC and the resulting spin correlation functions by using the Bogoliubov approximation. Section III presents numerical simulations of the dynamics of quenched BECs in 1D and 2D, and shows that spin vortices are indeed created due to the KZ mechanism in the present system. Section IV presents the conclusions of this paper.

II. BOGOLIUBOV ANALYSIS OF A QUENCHED FERROMAGNETIC BOSE-EINSTEIN CONDENSATE

A. Hamiltonian for spin-1 atoms

We consider spin-1 bosonic atoms with mass M confined in a potential $V_{\rm trap}(\boldsymbol{r})$. The noninteracting part of the Hamiltonian is given by

$$\hat{H}_0 = \int d\boldsymbol{r} \sum_{m=-1}^{1} \hat{\psi}_m^\dagger(\boldsymbol{r}) \left[-\frac{\hbar^2}{2M}\nabla^2 + V_{\rm trap}(\boldsymbol{r}) \right] \hat{\psi}_m(\boldsymbol{r}), \quad (1)$$

where $\hat{\psi}_m(\boldsymbol{r})$ annihilates an atom in a magnetic sublevel of spin $m=0,\pm 1$ at position $\boldsymbol{r}$.

The s-wave contact interaction between atoms is described by

$$\hat{H}_{\rm int} = \frac{1}{2}\int d\boldsymbol{r} :[c_0 \hat{\rho}^2(\boldsymbol{r}) + c_1 \hat{\boldsymbol{F}}^2(\boldsymbol{r})]:, \quad (2)$$

where the symbol :: indicates that the operators inside it are arranged in normal order and

$$\hat{\rho}(\boldsymbol{r}) = \sum_{m=-1}^{1} \hat{\psi}_m^\dagger(\boldsymbol{r})\hat{\psi}_m(\boldsymbol{r}), \quad (3)$$

$$\hat{\boldsymbol{F}}(\boldsymbol{r}) = \sum_{m,m'} \hat{\psi}_m^\dagger(\boldsymbol{r}) \boldsymbol{f}_{mm'} \hat{\psi}_{m'}(\boldsymbol{r}), \quad (4)$$

with $\boldsymbol{f}=(f_x,f_y,f_z)$ being the spin-1 matrices. The interaction coefficients in Eq. (2) are given by

$$c_0 = \frac{4\pi\hbar^2}{M}\frac{a_0+2a_2}{3}, \quad (5a)$$

$$c_1 = \frac{4\pi\hbar^2}{M}\frac{a_2-a_0}{3}, \quad (5b)$$

where a_S is the s-wave scattering length for two colliding atoms with total spin S.

When a magnetic field $\boldsymbol{B}$ is applied, the linear Zeeman effect rotates the spin around the direction of $\boldsymbol{B}$ at the Larmor frequency. Since $\hat{H}_0$ and $\hat{H}_{\rm int}$ are invariant with respect to rotation in spin space and we assume a uniform magnetic field, the linear Zeeman term has only a trivial effect on the spin dynamics, namely a uniform rotation of spins about $\boldsymbol{B}$. We therefore ignore the linear Zeeman effect by assuming that we are in a frame rotating in the spin space at the Larmor frequency. The quadratic Zeeman effect for an $F=1$ ^{87}Rb atom is described by

$$\hat{H}_q = \frac{\mu_{\rm B}^2}{4E_{\rm hf}}\int d\boldsymbol{r} \sum_{m,m'} \hat{\psi}_m^\dagger(\boldsymbol{r})[(\boldsymbol{B}\cdot\boldsymbol{f})^2]_{mm'}\hat{\psi}_{m'}(\boldsymbol{r}), \quad (6)$$

where $\mu_{\rm B}$ is the Bohr magneton and $E_{\rm hf}>0$ is the hyperfine splitting energy between $F=1$ and 2. The total Hamiltonian is given by the sum of Eqs. (1), (2), and (6):

$$\hat{H} = \hat{H}_0 + \hat{H}_q + \hat{H}_{\rm int}. \quad (7)$$

B. Time evolution in the Bogoliubov approximation

We consider now the spin dynamics of the system by using the Bogoliubov approximation with respect to an initial state in which all atoms are in the $m=0$ state. For simplicity, we assume $V_{\rm trap}=0$ in this section.

In the Bogoliubov approximation, the BEC part of the field operator is replaced by a c-number function. In the present case, we write the $m=0$ component of the field operator as

$$\hat{\psi}_0(\boldsymbol{r}) = e^{-ic_0 nt/\hbar}[\sqrt{n} + \delta\hat{\psi}_0(\boldsymbol{r})], \quad (8)$$

where n is the atomic density. We expand $\hat{\psi}_{\pm 1}(\boldsymbol{r})$ as

$$\hat{\psi}_{\pm 1}(\boldsymbol{r}) = e^{-ic_0 nt/\hbar}\sum_{\boldsymbol{k}} \frac{1}{\sqrt{V}} e^{i\boldsymbol{k}\cdot\boldsymbol{r}}\hat{a}_{\pm 1,\boldsymbol{k}}, \quad (9)$$

where V is the volume of the system and $\hat{a}_{\pm 1,\boldsymbol{k}}$ is the annihilation operator of an atom in the $m=\pm 1$ state with wave vector $\boldsymbol{k}$. Keeping terms up to the second order of $\delta\hat{\psi}_0(\boldsymbol{r})$ and $\hat{\psi}_{\pm 1}(\boldsymbol{r})$ in the Hamiltonian, we obtain the Heisenberg equations of motion for $\hat{a}_{\pm 1,\boldsymbol{k}}$ as

$$i\hbar\frac{d\hat{a}_{\pm 1,\boldsymbol{k}}(t)}{dt} = (\varepsilon_k + q + c_1 n)\hat{a}_{\pm 1,\boldsymbol{k}}(t) + c_1 n \hat{a}_{\mp 1,-\boldsymbol{k}}^\dagger(t), \quad (10)$$

where $\varepsilon_k=\hbar^2k^2/(2M)$ and $q=\mu_{\rm B}^2B^2/(4E_{\rm hf})$ with the assumption that the magnetic field is applied in the z direction. The solutions to Eq. (10) are obtained as

$$\hat{a}_{\pm 1,\boldsymbol{k}}(t) = \left(\cos\frac{E_k t}{\hbar} - i\frac{\varepsilon_k + q + c_1 n}{E_k}\sin\frac{E_k t}{\hbar}\right)\hat{a}_{\pm 1,\boldsymbol{k}}(0) - \left(i\frac{c_1 n}{E_k}\sin\frac{E_k t}{\hbar}\right)\hat{a}_{\mp 1,-\boldsymbol{k}}^\dagger(0), \quad (11)$$

where

$$E_k = \sqrt{(\varepsilon_k + q)(\varepsilon_k + q + 2c_1 n)}. \quad (12)$$

When E_k is imaginary, the corresponding modes are dynamically unstable and grow exponentially. Since $c_1<0$ and $q>0$ for $F=1$ ^{87}Rb atoms, exponential growth occurs for

$$q < 2|c_1|n \equiv q_{\rm c}. \quad (13)$$

The critical value $q_{\rm c}$ agrees with the phase boundary between the polar phase and the broken-axisymmetry phase [17,18]. When $q\leq q_{\rm c}/2$, the wave number of the most unstable mode is

$$k_{\rm mu} = \pm\sqrt{\frac{2M}{\hbar^2}\left(\frac{q_{\rm c}}{2} - q\right)}, \quad (14)$$

and $k_{\rm mu}=0$ when $q_{\rm c}/2<q<q_{\rm c}$. Due to the linearization in Eq. (10), the Bogoliubov approximation breaks down when the amplitudes of the unstable modes become large. The following analysis in this section is therefore applicable only for the initial stage of magnetization.

C. Instantaneous quench

We consider a situation in which q is much larger than the ferromagnetic energy $|c_1|n$ for $t<0$, and q is suddenly

quenched to below q_c at $t=0$. During the period of $t<0$, the time evolution in Eq. (11) is $\hat{a}_{\pm 1,\boldsymbol{k}}(t) \simeq e^{-iqt/\hbar}\hat{a}_{\pm 1,\boldsymbol{k}}(0)$, and the $m=\pm 1$ components remain in the vacuum state. For $t>0$, we obtain the time evolution of the density of the $m=\pm 1$ components as

$$\langle \hat{\psi}^{\dagger}_{\pm 1}(\boldsymbol{r},t)\hat{\psi}_{\pm 1}(\boldsymbol{r},t)\rangle = \frac{1}{V}\sum_{\boldsymbol{k}} \left| \frac{c_1 n}{E_k} \sin\frac{E_k t}{\hbar} \right|^2 \simeq \frac{1}{V}\sum_{k<k_c} \frac{q_c^2}{16|E_k|^2} e^{2|E_k|t/\hbar}, \tag{15}$$

where the expectation value is taken with respect to the vacuum state of the $m=\pm 1$ components. In the second line of Eq. (15), we have retained the unstable modes alone with $k < k_c \equiv \sqrt{2M(q_c-q)}/\hbar$ by assuming that $|E_k|t/\hbar \gg 1$. This result indicates that the number of atoms in the $m=\pm 1$ components grow exponentially after the quench.

Since the operator $\hat{\psi}_0$ in Eq. (4) is replaced by $\sqrt{n}$ in the Bogoliubov approximation, the magnetization operator $\hat{F}_+ = \hat{F}^{\dagger}_- = \hat{F}_x + i\hat{F}_y$ takes the form

$$\hat{F}_+(\boldsymbol{r}) = \sqrt{2n}[\hat{\psi}^{\dagger}_1(\boldsymbol{r}) + \hat{\psi}_{-1}(\boldsymbol{r})]. \tag{16}$$

Using Eq. (11), the time evolution of the correlation function is calculated to be

$$\langle \hat{F}_+(\boldsymbol{r},t)\hat{F}_-(\boldsymbol{r}',t)\rangle = \frac{2n}{V}\sum_{\boldsymbol{k}} \left| \cos\frac{E_k t}{\hbar} + i\frac{\varepsilon_k + q}{E_k}\sin\frac{E_k t}{\hbar} \right|^2 e^{i\boldsymbol{k}\cdot(\boldsymbol{r}-\boldsymbol{r}')} \tag{17a}$$

$$\simeq \frac{n}{2V}\sum_{k<k_c} \frac{q_c}{q_c - q - \varepsilon_k} e^{2|E_k|t/\hbar + i\boldsymbol{k}\cdot(\boldsymbol{r}-\boldsymbol{r}')}, \tag{17b}$$

where in the second line we have retained only the unstable modes.

The exponential factor in Eq. (17b) shows that the largest contribution to the sum is $\boldsymbol{k}$ around the mode with maximum $|E_k|$. The denominator in the summand of Eq. (17b) is much smoother than the exponential factor if q is not close to q_c, and therefore we can approximate ε_k with $\varepsilon_{\mathrm{mu}} = \hbar^2 k_{\mathrm{mu}}^2/(2M)$ in the denominator. We expand $2|E_k|t/\hbar$ around k_{mu} in the exponent as

$$\frac{2|E_k|t}{\hbar} = \frac{t}{\tau}\left(1 - \frac{1}{4}\xi_{\mathrm{corr}}^2 \Delta k^2 - \frac{1}{256}\Xi_{\mathrm{corr}}^4 \Delta k^4\right) + O(\Delta k^6), \tag{18}$$

where $\Delta k = k - k_{\mathrm{mu}}$; the expansion coefficients τ, ξ_{corr}, and Ξ_{corr} will be given below. It is clear that τ sets the time scale for exponential growth. Magnetization can be observed when it has grown sufficiently, i.e., after time $t \sim \tau$ has elapsed. Replacing the summation with the Gaussian integral in Eq. (17b), we find that ξ_{corr} represents the correlation length. For $q < q_c/2$, k_{mu} is given by Eq. (14), and

$$\tau = \frac{\hbar}{q_c}, \tag{19}$$

$$\xi_{\mathrm{corr}} = \sqrt{\frac{8\hbar^2}{M}\frac{q_c - 2q}{q_c^2}}. \tag{20}$$

For $q_c/2 < q < q_c$, $k_{\mathrm{mu}}=0$ and

$$\tau = \frac{\hbar}{2\sqrt{q(q_c - q)}}, \tag{21}$$

$$\xi_{\mathrm{corr}} = \sqrt{\frac{\hbar^2}{M}\frac{2q - q_c}{q(q_c - q)}}. \tag{22}$$

At $q=q_c/2$, Eqs. (20) and (22) vanish, and the Δk^4 term in Eq. (18) becomes important, with

$$\Xi_{\mathrm{corr}} = 4\left(\frac{\hbar^4}{2M^2 q_c^2}\right)^{1/4}. \tag{23}$$

We first consider a 1D system with a periodic boundary condition, i.e., a 1D-ring geometry. We assume that the radius of the ring R is much larger than the domain size, and that the curvature of the ring does not affect the dynamics. For $q < q_c/2$, the magnetic correlation function is calculated to be

$$\langle \hat{F}_+(\theta,t)\hat{F}_-(\theta',t)\rangle = \frac{2n}{\xi_{\mathrm{corr}}}\sqrt{\frac{\tau}{\pi t}}\cos[k_{\mathrm{mu}}R(\theta-\theta')]e^{t/\tau - \tau R^2(\theta-\theta')^2/(t\xi_{\mathrm{corr}}^2)}, \tag{24}$$

where τ and ξ_{corr} are given by Eqs. (19) and (20), and θ and θ' are azimuthal angles. For $q_c/2 < q < q_c$, we obtain

$$\langle \hat{F}_+(\theta,t)\hat{F}_-(\theta',t)\rangle = \frac{n}{2\xi_{\mathrm{corr}}}\sqrt{\frac{\tau}{\pi t}}\frac{q_c}{q_c - q}e^{t/\tau - \tau R^2(\theta-\theta')^2/(t\xi_{\mathrm{corr}}^2)}, \tag{25}$$

where τ and ξ_{corr} are given by Eqs. (21) and (22). At $q = q_c/2$, the correlation function reads

$$\langle \hat{F}_+(\theta,t)\hat{F}_-(\theta',t)\rangle = \frac{n}{2\pi\Xi_{\mathrm{corr}}}\frac{q_c}{q_c - q}\left(\frac{\tau}{t}\right)^{1/4} e^{t/\tau}\left[\Gamma\left(\frac{1}{4}\right){}_0F_2\left(\frac{1}{2},\frac{3}{4},\frac{\tau R^4(\theta-\theta')^4}{t\Xi_{\mathrm{corr}}^4}\right) - 8\sqrt{\frac{\tau}{t}}\frac{R^2(\theta-\theta')^2}{\Xi_{\mathrm{corr}}^2}\Gamma\left(\frac{3}{4}\right){}_0F_2\left(\frac{5}{4},\frac{3}{2},\frac{\tau R^4(\theta-\theta')^4}{t\Xi_{\mathrm{corr}}^4}\right)\right], \tag{26}$$

where Γ is the gamma function and

$$ {}_0F_2(a,b,z) = \sum_{j=0}^{\infty} \frac{\Gamma(a)\Gamma(b)}{\Gamma(a+j)\Gamma(b+j)} \frac{z^n}{j!} \tag{27} $$

is the generalized hypergeometric function.

We next consider the 2D geometry. For $q_c/2 < q < q_c$, for which $k_{mu}=0$, the integral resulting from Eq. (17b) can be performed analytically, giving

$$ \langle \hat{F}_+(\boldsymbol{r},t)\hat{F}_-(\boldsymbol{r}',t)\rangle = \frac{n\tau}{2\pi\xi_{corr}^2 t}\frac{q_c}{q_c-q} e^{t/\tau-\tau|\boldsymbol{r}-\boldsymbol{r}'|^2/(t\xi_{corr}^2)}, \tag{28} $$

where τ and ξ_{corr} are given by Eqs. (21) and (22). For other q, we can perform only the angular integral, giving

$$ \langle \hat{F}_+(\boldsymbol{r},t)\hat{F}_-(\boldsymbol{r}',t)\rangle = \frac{n}{4\pi}\frac{q_c}{q_c-q-\varepsilon_{mu}} \times \int_0^{\infty} kJ_0(k|\boldsymbol{r}-\boldsymbol{r}'|)e^{2|E_k|t/\hbar}dk, \tag{29} $$

where J_0 is the Bessel function. If the exponential factor is much sharper than the Bessel function around k_{mu}, the correlation function (29) can be approximated to be $\propto J_0(k_{mu}|\boldsymbol{r}-\boldsymbol{r}'|)$ [14,15].

As already shown, correlation function (17b) has a finite correlation length, and magnetizations at positions widely separated from each other grow in independent directions on the x-y plane. Thus the growth of the magnetic domains can be expected to generate topological defects through the KZ mechanism.

D. Slow quench

In the preceding sections, we have assumed that the magnetic field is suddenly quenched to the desired value at $t=0$ and that q is held constant for $t>0$. We assume here that for $t>0$ the magnetic field is quenched as

$$ q(t) = q_c\left(1-\frac{t}{\tau_Q}\right). \tag{30} $$

In the rest of this section, we consider only the case of $t < \tau_Q$.

The spin correlation can be estimated to be

$$ \langle \hat{F}_+(\boldsymbol{r},t)\hat{F}_-(\boldsymbol{r}',t)\rangle \propto \int d\boldsymbol{k}\, \exp\left[\int_0^t \frac{2|E_k(t')|t'}{\hbar}dt' + i\boldsymbol{k}\cdot(\boldsymbol{r}-\boldsymbol{r}')\right]. \tag{31} $$

Since we are interested in the vicinity of the critical point where the correlation starts to grow, we can expand $|E_k(t)|$ around $k_{mu}=0$ and keep the terms up to the order of k^2. For the 1D ring, we obtain

$$ \langle \hat{F}_+(\theta,t)\hat{F}_-(\theta',t)\rangle \propto e^{f(t)-R^2(\theta-\theta')^2/\xi_Q^2}. \tag{32} $$

For the 2D geometry, we obtain

$$ \langle \hat{F}_+(\boldsymbol{r},t)\hat{F}_-(\boldsymbol{r}',t)\rangle \propto e^{f(t)-|\boldsymbol{r}-\boldsymbol{r}'|^2/\xi_Q^2}, \tag{33} $$

where

$$ f(t) = \frac{\tau_Q q_c}{2\hbar}\left[\tan^{-1}\sqrt{\frac{t}{\tau_Q-t}} - \sqrt{\frac{t}{\tau_Q}\left(1-\frac{t}{\tau_Q}\right)}\left(1-\frac{2t}{\tau_Q}\right)\right], \tag{34} $$

$$ \xi_Q = \left[\frac{4\hbar}{M}\sqrt{t(\tau_Q-t)}\right]^{1/2}. \tag{35} $$

For $t \ll \tau_Q$, $f(t)$ can be expanded as

$$ f(t) = \frac{\tau_Q q_c}{2\hbar}\left[\frac{8}{3}\frac{t^{3/2}}{\tau_Q^{3/2}} + O\left(\frac{t^{5/2}}{\tau_Q^{5/2}}\right)\right], \tag{36} $$

and the time scale for magnetization is determined by setting $f(t)\sim 1$, giving

$$ t_Q \sim \left(\frac{\hbar}{q_c}\right)^{2/3}\tau_Q^{1/3}. \tag{37} $$

For the approximation in Eq. (36) to be valid, this t_Q must be much smaller than τ_Q, and therefore τ_Q must be much larger than $\hbar/q_c$. Substituting t_Q in Eq. (37) into Eq. (35) yields

$$ \xi_Q \sim \left(\frac{\hbar^4}{M^3 q_c}\right)^{1/6}\tau_Q^{1/3}. \tag{38} $$

The same power law is obtained in Ref. [14].

It is interesting to note that the results of (37) and (38) can also be obtained by Zurek's simple argument [2]. Since $q(t)$ depends on time, τ and ξ_{corr} given by Eqs. (21) and (22) are time-dependent, and hence they may be regarded as the growth time and correlation length at each instant of time. The local magnetization is developed after time t_Q has elapsed such that

$$ \tau(t_Q) \sim t_Q. \tag{39} $$

Using

$$ \tau(t) = \frac{\hbar\tau_Q}{2q_c\sqrt{t(\tau_Q-t)}} \simeq \frac{\hbar\sqrt{\tau_Q}}{2q_c\sqrt{t}}, \tag{40} $$

we can obtain t_Q in Eq. (37). Substituting this t_Q into

$$ \xi_{corr}^2(t) = \frac{\hbar^2}{Mq_c}\frac{\tau_Q-2t}{t(\tau_Q-t)} \simeq \frac{\hbar^2\tau_Q}{Mq_c t}, \tag{41} $$

we obtain Eq. (38).

III. NUMERICAL SIMULATIONS AND THE KIBBLE-ZUREK MECHANISM

A. Gross-Pitaevskii equation with random initial seeds

The multicomponent Gross-Pitaevskii (GP) equation is obtained by replacing the field operator $\hat{\psi}_m$ with the macroscopic wave function ψ_m in the Heisenberg equation of motion:

$$i\hbar\frac{\partial\psi_{\pm1}}{\partial t}=\left(-\frac{\hbar^2}{2M}\nabla^2+V_{\rm trap}+q+c_0\rho\right)\psi_{\pm1}+c_1\left(\frac{1}{\sqrt{2}}F_{\mp}\psi_0\pm F_z\psi_{\pm1}\right),\tag{42a}$$

$$i\hbar\frac{\partial\psi_0}{\partial t}=\left(-\frac{\hbar^2}{2M}\nabla^2+V_{\rm trap}+c_0\rho\right)\psi_0+\frac{c_1}{\sqrt{2}}(F_+\psi_1+F_-\psi_{-1}),\tag{42b}$$

where ρ and $\boldsymbol{F}$ are defined by using ψ_m instead of $\hat{\psi}_m$ in Eqs. (3) and (4). The wave function is normalized as

$$\int d\boldsymbol{r}\sum_{m=-1}^{1}|\psi_m|^2=N,\tag{43}$$

with N being the total number of atoms in the condensate.

Suppose that all atoms are initially in the $m=0$ state. It then follows from Eq. (42a) that $\psi_{\pm1}$ will remain zero in the subsequent time evolution. This is because quantum fluctuations in the transverse magnetization that trigger the growth of magnetization are ignored in the mean-field approximation. We therefore introduce appropriate initial noise in $\psi_{\pm1}$ so that the dynamics of spontaneous magnetization can be studied using mean-field theory.

We write the initial state as

$$\psi_{\pm1}(\boldsymbol{r})=\sum_{\boldsymbol{k}}\frac{1}{\sqrt{V}}e^{i\boldsymbol{k}\cdot\boldsymbol{r}}a_{\pm1,\boldsymbol{k}}(0),\tag{44}$$

where $a_{\pm1,\boldsymbol{k}}$ are c-numbers. We assume that the c-number amplitudes $a_{\pm1,\boldsymbol{k}}(0)$ are stochastic variables whose average values vanish, i.e.,

$$\langle a_{\pm1,\boldsymbol{k}}(0)\rangle_{\rm avg}=0,\tag{45}$$

where $\langle\cdots\rangle_{\rm avg}$ denotes the statistical average over an appropriate probability distribution. The linear approximation to the GP equation with respect to $a_{\pm1,\boldsymbol{k}}$ gives the same time evolution as Eq. (11), in which the operators are replaced by the c-numbers. The spin correlation function is then obtained by

$$\begin{aligned}\langle F_+(\boldsymbol{r},t)F_-(\boldsymbol{r}',t)\rangle_{\rm avg}&=\frac{2n}{V}\sum_{\boldsymbol{k}}\left|\cos\frac{E_kt}{\hbar}+i\frac{\varepsilon_k+q}{E_k}\sin\frac{E_kt}{\hbar}\right|^2\\&\times[e^{-i\boldsymbol{k}\cdot(\boldsymbol{r}-\boldsymbol{r}')}\langle|a_{1,\boldsymbol{k}}(0)|^2\rangle_{\rm avg}\\&+e^{i\boldsymbol{k}\cdot(\boldsymbol{r}-\boldsymbol{r}')}\langle|a_{-1,-\boldsymbol{k}}(0)|^2\rangle_{\rm avg}].\end{aligned}\tag{46}$$

Comparing Eq. (46) with Eq. (17a), we find that they coincide if the mean squared averages of $a_{\pm1,\boldsymbol{k}}(0)$ satisfy

$$\langle|a_{1,\boldsymbol{k}}(0)|^2\rangle_{\rm avg}+\langle|a_{-1,\boldsymbol{k}}(0)|^2\rangle_{\rm avg}=1\tag{47}$$

for all $\boldsymbol{k}$. Since $m=+1$ and -1 should be symmetric for the present initial state, we have

$$\langle|a_{\pm1,\boldsymbol{k}}(0)|^2\rangle_{\rm avg}=\frac{1}{2}.\tag{48}$$

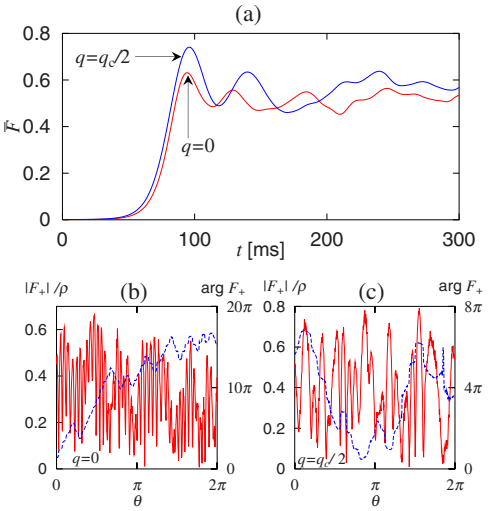

FIG. 1. (Color online) (a) Time evolution of the autocorrelation function given by Eq. (50) for an instantaneous quench to $q=0$ and $q=q_c/2$ with 1D ring geometry. (b) Magnitude of the normalized magnetization $|F_+|/\rho$ (solid curve, left axis) and direction of the magnetization arg F_+ (dashed curve, right axis) at $t=70$ ms for $q=0$ and (c) for $q=q_c/2$. The radius of the ring is $R=50$ μm, the atomic density is $n=2.8\times10^{14}$ cm^{-3}, and the number of atoms is $N=10^6$.

In the following, we perform numerical simulations of spontaneous magnetization by using the GP equation with initial conditions (45) and (48) and show that the ensuing dynamics exhibit defect formation similar to the KZ mechanism. More specifically, we use Eq. (44) with

$$a_{\pm1,\boldsymbol{k}}(0)=\alpha_{\rm rnd}+i\beta_{\rm rnd},\tag{49}$$

where $\alpha_{\rm rnd}$ and $\beta_{\rm rnd}$ are random variables following the normal distribution $p(x)=\sqrt{2/\pi}\exp(-2x^2)$. Equation (49) then satisfies Eqs. (45) and (48).

B. 1D-ring geometry

Let us first investigate the 1D-ring system. This geometry can be experimentally achieved, e.g., by an optical trap using a Laguerre-Gaussian beam [19]. We can reduce the GP equation (42a) and (42b) to 1D by assuming that the wave function ψ_m depends only on the azimuthal angle θ. The average density of atoms is assumed to be $n=2.8\times10^{14}$ cm^{-3}. When the radius R of the ring is 50 μm and the radius of the small circle is 2 μm, the total number of atoms is $N\simeq10^6$.

Figure 1 presents single runs of time evolution for the initial state given by Eqs. (44) and (49). Figure 1(a) shows the time evolution of the normalized autocorrelation function defined by

$$\bar{F}(t)=\int Rd\theta\frac{|F_+(\theta,t)|^2}{\rho^2(\theta,t)}.\tag{50}$$

For both $q=0$ and $q=q_c/2$, the transverse magnetization grows exponentially with a time constant $\sim\tau=\hbar/q_c\simeq8$ ms. Snapshots of the transverse magnetization at $t=70$ ms are shown in Figs. 1(b) and 1(c) for $q=0$ and $q=q_c/2$, respec-

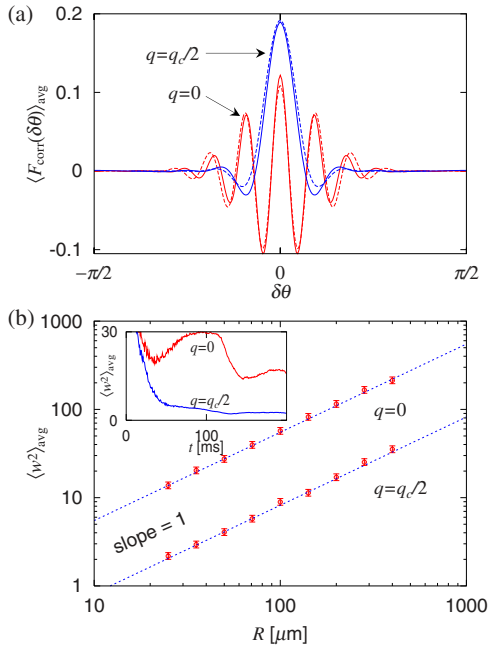

FIG. 2. (Color online) (a) Numerically obtained correlation function defined by Eq. (52) at $t=70$ ms after q is instantaneously quenched to $q=0$ and $q=q_c/2$ (solid curves). The dashed curves are theoretical fits using Eqs. (24) and (26). The parameters are the same as those in Fig. 1. (b) Dependence of the variance of the spin winding number on the radius of the ring R at $t=70$ ms. The number of atoms is related to R as $N=10^6\times R[\mu\text{m}]/50$. The dashed lines are proportional to R. The inset shows the time dependence of $\langle w^2\rangle_{\rm avg}$ for $R=50$ μm, where only $\langle w^2\rangle_{\rm avg}<30$ is shown since the random initial phases make the winding numbers huge. The data in (a) and (b) are averages over 1000 runs of simulations for different initial states produced by random numbers. The error bars in (b) represent the 95% confidence interval of the χ^2 distribution.

tively. We define the spin winding number w to be an integer representing the number of rotations of the spin vector in the x-y plane along the circumference of the ring:

$$w=\frac{1}{2\pi}\int_0^{2\pi} Rd\theta\frac{1}{2i|F_+|^2}\left(F_-\frac{\partial F_+}{\partial\theta}-F_+\frac{\partial F_-}{\partial\theta}\right). \tag{51}$$

The spin winding numbers are $w=7$ in Fig. 1(b) and $w=-1$ in Fig. 1(c).

Figure 2 shows the ensemble average of the normalized correlation function,

$$\langle F_{\rm corr}(\delta\theta)\rangle_{\rm avg}=\left\langle\frac{\int d\theta F_+(\theta)F_-(\theta+\delta\theta)}{\int d\theta\rho(\theta)\rho(\theta+\delta\theta)}\right\rangle_{\rm avg}, \tag{52}$$

and the variance of the winding number at $t=70$ ms. The ensemble average of the winding number, $\langle w\rangle_{\rm avg}$, vanishes due to the random nature of the initial noise, and the standard deviation, $\langle w^2\rangle_{\rm avg}^{1/2}$, should be regarded as a typical winding number. The variance is expected to obey the χ^2 distribution with 1000 degrees of freedom, which is equal to the number of runs of simulations to take each data point, and hence we show the 95% confidence interval to estimate the statistical errors in Fig. 2. For an ensemble average of 100 runs, the length of the error bars in a logarithmic plot would become about three times larger than that for 1000 runs.

We can see that $\langle F_{\rm corr}(\delta\theta)\rangle_{\rm avg}$ [solid curves in Fig. 2(a)] agrees well with the correlation functions in Eqs. (24) and (26) that are obtained by the Bogoliubov analysis [dashed curves in Fig. 2(a)]. For $q=q_c/2$, the correlation function has a characteristic width of $\sim\Xi_{\rm corr}$ in Eq. (23), indicating that the ring is filled with magnetic domains with an average size of $\sim\Xi_{\rm corr}$. According to the KZ theory, the magnetic domains with random directions give rise to the spin winding, which is estimated to be $w\sim(R/\Xi_{\rm corr})^{1/2}$. This R dependence of w is clearly seen in Fig. 2(b). The winding numbers in Fig. 2(b) must be determined after magnetization has become well-developed ($t\gtrsim 50$ ms) and before the Bogoliubov approximation breaks down ($t\lesssim 100$ ms) to obtain the power law.

The situation is different for $q=0$, in which the correlation function oscillates within a Gaussian envelope, as shown in Fig. 2(a). The oscillatory behavior of the correlation function gives a clue as to how the KZ mechanism manifests itself in a spin-conserving system. The finite correlation length for $q=0$ indicates that the spin is conserved not only globally but also locally; that is, the spin integrated over the correlation length $\xi_{\rm corr}$,

$$\int_{|\delta\boldsymbol{r}|\le\xi_{\rm corr}}\boldsymbol{F}(\boldsymbol{r}+\delta\boldsymbol{r})d\delta\boldsymbol{r}, \tag{53}$$

is zero for any $\boldsymbol{r}$. Thus the neighboring domains tend to have opposite magnetizations to locally cancel out the spin, so that domains far from each other can grow independently; the spin conservation and the KZ postulate of independent growth of separated domains are thus compatible.

The spin winding for $q<q_c/2$ is attributed to both the KZ mechanism and dynamical instability. The oscillation in the correlation function originates from the fact that the most unstable modes have nonzero wave numbers $\pm k_{\rm mu}$. Each correlated region of size $\sim\xi_{\rm corr}=[8\hbar^2/(Mq_c)]^{1/2}$ contains spin waves of $e^{ik_{\rm mu}R\theta}$ and $e^{-ik_{\rm mu}R\theta}$. If there is an imbalance between amplitudes of these modes, the winding number monotonically increases or decreases in each region of $\sim\xi_{\rm corr}$. This is why $\langle w^2\rangle_{\rm avg}$ is larger for $q=0$ than for $q=q_c/2$ in Fig. 2(b). It follows from this consideration that for $k_{\rm mu}\xi_{\rm corr}\gg 1$ the winding number is proportional to

$$k_{\rm mu}\xi_{\rm corr}\sqrt{\frac{R}{\xi_{\rm corr}}}=k_{\rm mu}\sqrt{R\xi_{\rm corr}}\propto\left(1-\frac{2q}{q_c}\right)^{3/4}, \tag{54}$$

where Eqs. (14) and (20) are used. Figure 3 shows the variance of the winding number versus $1-2q/q_c$. For small q, $\langle w^2\rangle_{\rm avg}$ is proportional to $(1-2q/q_c)^{3/2}$, in agreement with Eq. (54). When q is close to $q_c/2$, the spin winding within the correlated region, $k_{\rm mu}\xi_{\rm corr}$, becomes small, and then the winding number reduces to the value shown in Fig. 2(b), i.e., $\langle w^2\rangle_{\rm avg}\simeq 4$.

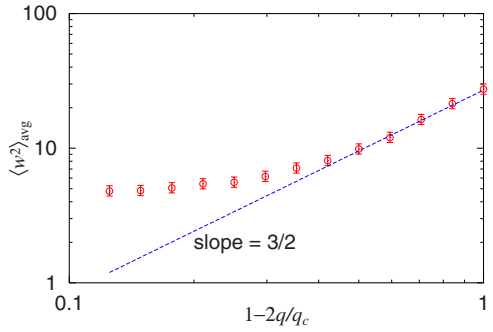

FIG. 3. (Color online) Dependence of the variance of the spin winding number w on quadratic Zeeman energy q. The winding number is calculated as $t=70$ ms after an instantaneous quench. The parameters are the same as those in Fig. 1 except for q. The dashed line is proportional to $(1-2q/q_c)^{3/2}$. The plots show the averages over 1000 runs of simulations for different initial states produced by random numbers. The error bars represent the 95% confidence interval of the χ^2 distribution.

We next discuss the results of simulations for the quench process given in Eq. (30). Since the winding number for a slow quench is small compared with that for an instantaneous quench, we take a large ring of $R=400$ μm. Following the scaling law in Eq. (37), we take the winding number at

$$t = c\left(\frac{\hbar}{q_c}\right)^{2/3}\tau_Q^{1/3} \tag{55}$$

with $c=4$ for various quench times τ_Q. Figure 4 shows the variance of the winding number as a function of the quench time. We can clearly see that $\langle w^2\rangle_{\rm avg}$ has a power law of $\tau_Q^{-1/3}$

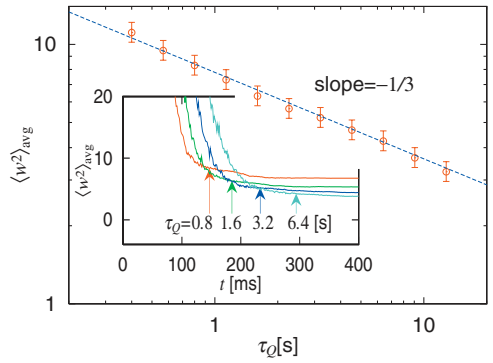

FIG. 4. (Color) Dependence of the variance of the spin winding number on quench time τ_Q, where q is quenched according to Eq. (30). The time at which each plot is taken depends on τ_Q as $t=4\tau_Q^{1/3}(\hbar/q_c)^{2/3}$, as shown by the arrows in the inset. The radius of the ring is $R=400$ μm, the atomic density is $n=2.8\times10^{14}$ cm^{-3}, and the number of atoms is $N=8\times10^6$. The dashed line is proportional to $\tau_Q^{-1/3}$. The inset shows the time evolution of $\langle w^2\rangle_{\rm avg}$, where only $\langle w^2\rangle_{\rm avg}<20$ is shown since the random initial phases make the winding numbers huge. The data are averages over 1000 runs of simulations for the different initial states produced by random numbers. The error bars represent the 95% confidence interval of the χ^2 distribution.

within the range of statistical error, which is in agreement with $\xi_Q^{-1}\sim\tau_Q^{-1/3}$, with ξ_Q given by Eq. (38). Thus the present system follows the quench-time scaling law of Zurek [2].

The winding number converges to an almost constant value, as shown in the inset of Fig. 4. This is because the phase profile formed at $t\sim t_Q$ is roughly maintained owing to the small value of the excess kinetic energy for a slow quench. Therefore even if we take the winding number at a fixed time, for example, $t=400$ ms in the case of Fig. 4, the winding number follows the same power law as that in Fig. 4 (data not shown). This is in contrast with the case of an instantaneous quench, in which the typical winding number changes with time [see the inset of Fig. 2(b)], since the ferromagnetic energy is converted to kinetic energy and the system exhibits complicated dynamics after the growth of magnetization.

C. 2D-disk geometry

When the confinement in the z direction is sufficiently tight, the system behaves effectively two-dimensionally. For simplicity, we ignore the density dependence in the z direction and assume that the 2D GP equation has the same form as Eqs. (42a) and (42b). We assume that the wave function vanishes at the wall located at $(x^2+y^2)^{1/2}=R_w=100$ μm, and that the potential is flat inside the wall. The density $n=2.8\times10^{14}$ cm^{-3} is then almost constant, except within the healing length $\{3/[8\pi n(a_0+2a_2)]\}^{1/2}\simeq0.16$ μm near the wall. When the thickness in the z direction is $\simeq1$ μm, the number of atoms is $N\simeq10^7$. Such a system can be achieved by using an optical sheet and a hollow laser beam.

The initial state of ψ_0 is a stationary solution of the GP equation, and the initial state of $\psi_{\pm1}$ is given by Eq. (44) with random variables (49). Figure 5(a) shows the time evolution of the autocorrelation function for transverse magnetization,

$$\bar{F}(t) = \int d\boldsymbol{r}\frac{|F_+(\boldsymbol{r},t)|^2}{\rho^2(\boldsymbol{r},t)}, \tag{56}$$

which grows exponentially with the same time constant as that in Fig. 1, and saturates for $t\gtrsim100$ ms.

Snapshots of $|F_+(\boldsymbol{r})|$ and $\arg F_+(\boldsymbol{r})$ at $t=100$ ms are shown in Figs. 5(b) and 5(c). We can see that $|F_+(\boldsymbol{r})|$ at $t\gtrsim100$ ms contains many holes, around which the spin direction rotates by 2π. Since this topological spin structure consists of singly-quantized vortices in the $m=\pm1$ states with its core filled by atoms in the $m=0$ state, it is called a polar-core vortex (the BEC in the $m=0$ state is called polar). We can estimate the spin healing length ξ_s by equating the kinetic energy $\hbar^2/(2M\xi_s^2)$ with the energy of magnetization $|q-q_c|$, giving

$$\xi_s = \frac{\hbar}{\sqrt{2M|q-q_c|}}. \tag{57}$$

This length scale is $\xi_s\simeq1.7$ μm for $q=0$ and $\xi_s\simeq2.4$ μm for $q=q_c/2$, which are in good agreement with the sizes of the vortex cores in Figs. 5(b) and 5(c).

In 2D, the correlation function is defined by

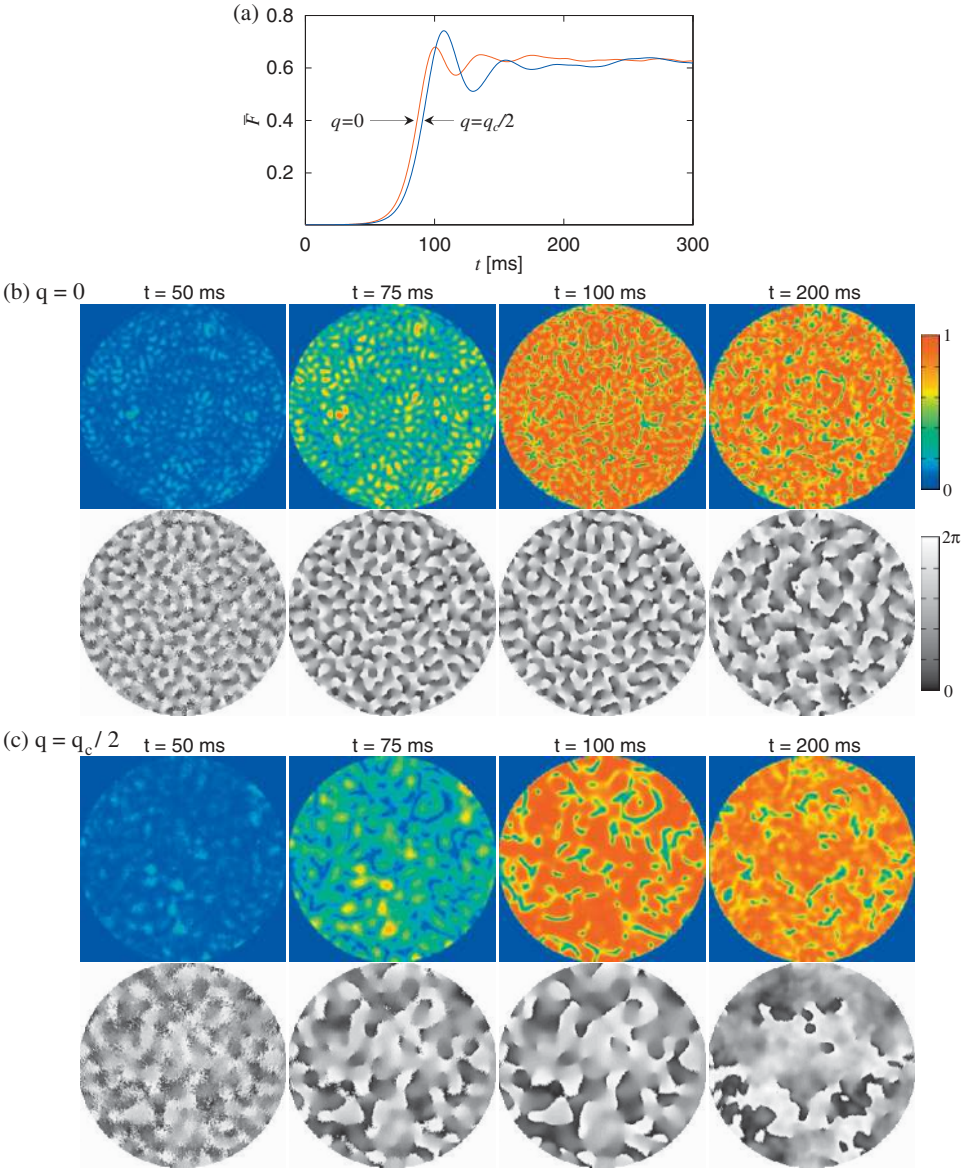

FIG. 5. (Color) (a) Time evolution of the autocorrelation function given by Eq. (56) for an instantaneous quench of q with 2D disk geometry. The radius of the disk is $R_w=100$ μm, the atomic density is $n=2.8\times10^{14}$ cm^{-3}, and the number of atoms is $N=10^7$. (b) Profiles of the magnetization $|F_+|$ (upper) and its direction arg F_+ (lower) for $q=0$ and (c) for $q=q_c/2$. The size of each panel is 200×200 μm^2.

$$\langle F_{\rm corr}(\delta \boldsymbol{r})\rangle_{\rm avg} = \left\langle \frac{\int d\boldsymbol{r} F_+(\boldsymbol{r}) F_-(\boldsymbol{r}+\delta\boldsymbol{r})}{\int d\boldsymbol{r}\rho(\boldsymbol{r})\rho(\boldsymbol{r}+\delta\boldsymbol{r})} \right\rangle_{\rm avg}, \quad (58)$$

which is shown in Figs. 6(a) and 6(b). We find that, as in the 1D case, the most unstable wavelength is reflected in the shape of the spin correlation function (58), and the characteristics of these correlation functions in the radial direction are similar to those in 1D shown in Fig. 2. For $q=0$, the mean distance between the spin vortices in Fig. 5(b) is not determined by the correlation length [which is equal to the width of the envelope of the concentric pattern in Fig. 6(a)] but by $\sim k_{\rm mu}^{-1}$, i.e., the width of the concentric rings in Fig. 6(a). On the other hand, for $q=q_c/2$, the density of the spin vortices is determined by the correlation length, i.e., the size of the blue circle $\simeq 30$ μm in Fig. 6(b). The staggered concentric correlation for $q=0$ suggests that the spin is locally conserved within the region of the correlation length, and domains at a distance larger than the correlation length grow independently, while conserving the total spin.

The spin winding number for 2D is defined as

$$w(R) = \frac{1}{2\pi}\oint_{C(R)} \frac{1}{2i|F_+|^2}(F_-\nabla F_+ - F_+\nabla F_-)d\boldsymbol{r}, \quad (59)$$

where $C(R)$ is a circle of radius $R<R_w$ located at the center of the system. Figure 6(c) shows the R dependence of the ensemble average of $w^2(R)$, where the radius of the system is fixed at $R_w=100$ μm and the data are taken at $t=100$ ms. It should be noted that $\langle w^2(R)\rangle_{\rm avg}$ is proportional to R for large R, as expected from the KZ theory [2], while it is proportional to R^2 for small R. This R^2 dependence is due to the fact that the probability P for a spin vortex to be in the circle is proportional to πR^2. The variance of the winding number is therefore $0(1-P)+1^2P/2+(-1)^2P/2\propto R^2$ if the probability of two or more vortices entering the circle is negligible. This condition is met when the density of the spin vortices multiplied by πR^2 is much smaller than unity, and hence the

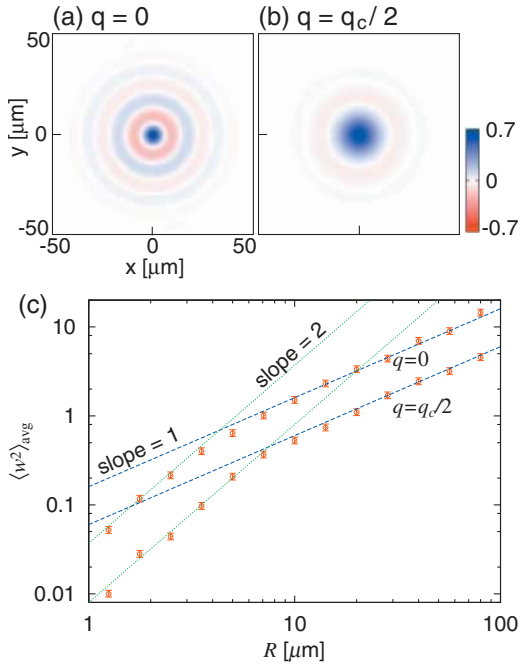

FIG. 6. (Color) (a) Spin correlation function defined by Eq. (58) at $t=100$ ms after q has been instantaneously quenched to $q=0$ and (b) to $q=q_c/2$. (c) Variance of the winding number along the circumference of a circle of radius R, where the data are taken at $t=100$ ms. The blue and green lines are, respectively, proportional to R and R^2. In (a)–(c) the parameters are the same as those in Fig. 5, and the data represent averages over 1000 runs of simulations for the different initial states produced by random numbers. The error bars in (c) represent the 95% confidence interval of the χ^2 distribution.

radius R at which the crossover from $\langle w^2(R)\rangle_{\rm avg} \propto R$ to $\propto R^2$ occurs is larger for $q=q_c/2$ than for $q=0$. As in the 1D case, nonzero $k_{\rm mu}$ enhances the winding of the magnetization, with the winding number being larger for $q=0$ than for $q=q_c/2$.

Figures 5(b) and 5(c) clearly show that the density of the spin vortices is uniform when the size of the system is large enough. The number of spin vortices within a radius R is therefore proportional to R^2. If the topological charge of each spin vortex, +1 or −1, was chosen at random, the net winding number along a circle of radius R, i.e., the difference between the number of +1 and −1 vortices, would be proportional to R. However, from Fig. 6(c), the winding number is proportional to $R^{1/2}$ for large R, consistent with the KZ theory. Thus the topological charges of nearby spin vortices are not random, but tend to anticorrelate with each other so as to reduce the net winding number.

Figure 7 shows the result of a slow quench for the 2D case, where $q(t)$ is given by Eq. (30). From Eq. (37), we specify the time at which the winding number is taken as Eq. (55) with $c=4$, as indicated by the arrows in the inset of Fig. 7. We can see that the winding number follows the scaling law, $\langle w^2\rangle_{\rm avg} \propto \tau_{\rm Q}^{-1/3}$, as predicted by Eq. (38), indicating that Zurek's discussion is also applicable to the 2D case.

In order to obtain the scaling law in Fig. 7, we must specify the time at which the winding number is taken, since the spin winding number gradually decays with time as

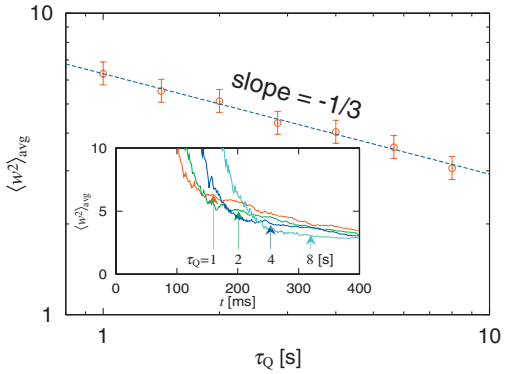

FIG. 7. (Color) (a) Variance of the spin winding number versus quench time $\tau_{\rm Q}$ for a 2D disk geometry, where q is quenched according to Eq. (30). The inset shows the time evolution of $\langle w^2\rangle_{\rm avg}$, where only $\langle w^2\rangle_{\rm avg}<10$ is shown since the random initial phases make the winding numbers huge. The time at which each plot is taken depends on $\tau_{\rm Q}$ as $t=4\tau_{\rm Q}^{1/3}(\hbar/q_c)^{2/3}$, as shown by the arrows in the inset. The dashed line is proportional to $\tau_{\rm Q}^{-1/3}$. The radius of the disk is $R_{\rm w}=400$ μm and the closed path for taking the winding number is $R=320$ μm. The atomic density is $n=2.8\times10^{14}$ cm^{-3} and the number of atoms is $N=1.6\times10^8$. The data are averages over 1000 runs of simulations for the different initial states produced by random numbers. The error bars represent the 95% confidence interval of the χ^2 distribution.

shown in the inset of Fig. 7, in contrast to the 1D case (inset of Fig. 4). Using Eq. (55) to specify the time, we can obtain the correct power law for $c\gtrsim 3$ and up to at least $c\simeq 6$. However, if we take the winding number at a fixed time or at a time proportional to $\tau_{\rm Q}$, the power law cannot be obtained.

IV. CONCLUSIONS

In this paper, we have studied the dynamics of a spin-1 BEC with a ferromagnetic interaction, after a quench of the applied magnetic field, in an effort to investigate spontaneous defect formation in a spinor BEC. We have analyzed the magnetization triggered by quantum fluctuations by using the Bogoliubov approximation and performed numerical simulations of the GP equation with initial conditions that simulate quantum fluctuations.

We have shown that the correlation functions for the magnetization have finite correlation lengths [Figs. 2, 6(a), and 6(b)], and therefore magnetic domains far from each other grow in random directions. We find that topological defects, i.e., spin vortices, emerge through the KZ mechanism. We have confirmed that the winding number along a closed path is proportional to the square root of the length of the path [Figs. 2(b) and 6(c)], indicating that topological defects are formed from domains with random directions of magnetizations.

Even when the total magnetization is conserved for $q=0$, the winding number is proportional to $R^{1/2}$, in agreement with the KZ theory [Fig. 2(b)]. This is due to the fact that domains within the correlation length tend to be aligned in such a manner as to cancel out the local magnetization. Thus the neighboring domains have local correlation, while the

domains far from each other are independent, which makes the KZ postulate of independent growth of widely separated domains compatible with the total spin conservation. The local spin correlation increases the winding number as in Eq. (54), which results in the q dependence of the winding number as shown in Fig. 3.

When the magnetic field is quenched in a finite time τ_Q as in Eq. (30), the winding number is found to be proportional to $\tau_Q^{-1/6}$ (Figs. 4 and 7). This τ_Q dependence of the winding number can be understood from Zurek's simple argument [2]: the domains are frozen when the spin relaxation time becomes of the same order as the time elapsed after the quench.

In the Berkeley experiment [12], the system had an elongated quasi-2D geometry, and is not suitable for testing the KZ mechanism. The KZ mechanism should apply to a system in which the dimension along the short axis (the x direction in Ref. [12]) is much larger. In this case, the harmonic potential may affect the scaling law, which merits further study. Moreover, from the analysis in Ref. [13], the experiment of Ref. [12] indicates that there are some initial atoms in the $m=\pm 1$ components with long-range correlation, which play the role of seeds for widely correlated domains and may hinder the observation of the KZ mechanism. If the residual atoms in the $m=\pm 1$ components are completely eliminated, magnetization is triggered by quantum fluctuations as shown in the present paper. Another way to remove the effect of the residual atoms may be by applying random phases to the $m=\pm 1$ states to erase the initial correlation.

Note added. Recently, Damski and Zurek [20] performed 1D simulations of the quench dynamics of a spin-1 BEC.

ACKNOWLEDGMENTS

This work was supported by Grants-in-Aid for Scientific Research (Grants No. 17740263 and No. 17071005) and by the 21st Century COE programs on "Coherent Optical Science" and "Nanometer-Scale Quantum Physics" from the Ministry of Education, Culture, Sports, Science and Technology of Japan. H. S. acknowledges support by the Matsuo Foundation.

[1] T. W. B. Kibble, J. Phys. A **9**, 1387 (1976).
[2] W. H. Zurek, Nature (London) **317**, 505 (1985); Phys. Rep. **276**, 177 (1996).
[3] I. Chuang, R. Durrer, N. Turok, and B. Yurke, Science **251**, 1336 (1991).
[4] M. J. Bowick, L. Chandar, E. A. Schiff, and A. M. Srivastava, Science **263**, 943 (1994).
[5] P. C. Hendry, N. S. Lawson, R. A. M. Lee, P. V. E. McClintock, and C. D. H. Williams, Nature (London) **368**, 315 (1994); M. E. Dodd, P. C. Hendry, N. S. Lawson, P. V. E. McClintock, and C. D. H. Williams, Phys. Rev. Lett. **81**, 3703 (1998).
[6] V. M. H. Ruutu, V. B. Eltsov, A. J. Gill, T. W. B. Kibble, M. Krusius, Yu. G. Makhlin, B. Plaçais, G. E. Volovik, and W. Xu, Nature (London) **382**, 334 (1996); V. M. Ruutu, V. B. Eltsov, M. Krusius, Yu. G. Makhlin, B. Plaçais, and G. E. Volovik, Phys. Rev. Lett. **80**, 1465 (1998).
[7] C. Bäuerle, Yu. M. Bunkov, S. N. Fisher, H. Godfrin, and G. R. Pickett, Nature (London) **382**, 332 (1996).
[8] S. Ducci, P. L. Ramazza, W. González-Viñas, and F. T. Arecchi, Phys. Rev. Lett. **83**, 5210 (1999).
[9] R. Carmi, E. Polturak, and G. Koren, Phys. Rev. Lett. **84**, 4966 (2000).
[10] R. Monaco, J. Mygind, and R. J. Rivers, Phys. Rev. Lett. **89**, 080603 (2002).
[11] A. Maniv, E. Polturak, and G. Koren, Phys. Rev. Lett. **91**, 197001 (2003).
[12] L. E. Sadler, J. M. Higbie, S. R. Leslie, M. Vengalattore, and D. M. Stamper-Kurn, Nature (London) **443**, 312 (2006).
[13] H. Saito, Y. Kawaguchi, and M. Ueda, Phys. Rev. A **75**, 013621 (2007).
[14] A. Lamacraft, Phys. Rev. Lett. **98**, 160404 (2007).
[15] M. Uhlmann, R. Schützhold, and U. R. Fischer, Phys. Rev. Lett. **99**, 120407 (2007).
[16] H. Saito, Y. Kawaguchi, and M. Ueda, Phys. Rev. Lett. **96**, 065302 (2006).
[17] J. Stenger, S. Inouye, D. M. Stamper-Kurn, H.-J. Miesner, A. P. Chikkatur, and W. Ketterle, Nature (London) **396**, 345 (1998).
[18] K. Murata, H. Saito, and M. Ueda, Phys. Rev. A **75**, 013607 (2007).
[19] T. Kuga, Y. Torii, N. Shiokawa, T. Hirano, Y. Shimizu, and H. Sasada, Phys. Rev. Lett. **78**, 4713 (1997).
[20] B. Damski and W. H. Zurek, Phys. Rev. Lett. **99**, 130402 (2007).